

1 Submarine channels “swept” downstream after bend cutoff in salt 2 basins

3
4 **Jacob A. Covault, Zoltán Sylvester, Michael R. Hudec, Can Ceyhan, and Dallas Dunlap**

5 *Bureau of Economic Geology, Jackson School of Geosciences, University of Texas at Austin,*
6 *Austin, TX 78713*

7 Corresponding author email: jake.covault@beg.utexas.edu

9 **ABSTRACT**

10 Channel-bend expansion and downstream translation, as well as vertical movements by
11 aggradation and incision, set the stratigraphic architecture of channelized depositional systems.
12 Early work on submarine-channel evolution has suggested that downstream translation is rare. We
13 propose that downstream translation of bends might be common in deep-water salt-tectonic
14 provinces, where complex topography can localize channel pathways that promote meander
15 cutoffs and the generation of high-curvature bends. We use three-dimensional seismic-reflection
16 data from a region with salt-influenced topography in the Campos basin, offshore Brazil, to
17 characterize the structural geometry of a salt diapir and stratigraphic architecture of an adjacent
18 ~18 km-long reach of a submarine-channel system. We interpret the structural and stratigraphic
19 evolution, including meander-cutoff development near the salt diapir followed by ~10 km of
20 downstream translation of a channel bend. We test the stratigraphic evolution with a simple
21 numerical model of channel meandering. This integrated subsurface characterization and
22 stratigraphic modeling study sheds light on the processes and controls of submarine-channel
23 downstream translation, which might be common in rapidly deforming settings, such as salt basins,
24 that promote localized subsidence, meander cutoffs, and rapidly translating, high-curvature bends.

25

26 **INTRODUCTION**

27 Submarine channels are conduits for sediment-gravity flows to deep water (Piper and
28 Normark, 2001), delivering sediment to the largest detrital accumulations on Earth in submarine
29 fans (Barnes and Normark, 1985). Submarine-channel deposits contain a record of deep-water
30 sediment dispersal (Hubbard et al., 2014) and changes in upstream source areas (Romans et al.,
31 2016) as well as form hydrocarbon reservoirs (Pettingill and Weimer, 2002) and store large
32 amounts of organic carbon (Galy et al., 2008). Submarine channels have been known since the
33 1980's to exhibit planform morphologic characteristics similar to rivers (e.g., Damuth et al., 1983);
34 however, some of the influential papers have stressed their unique migration style compared to
35 their fluvial counterparts (e.g., Peakall et al., 2000; Wynn et al., 2007). This is important because
36 channel migration, that is, the expansion and downstream translation of bends (i.e., “swing” and
37 “sweep”; Posamentier, 2003), as well as vertical movements by aggradation and incision, set the
38 stratigraphic architecture of channelized depositional systems (Sylvester et al., 2011; Jobe et al.,
39 2016). For example, combined translation and expansion of river bends, with little aggradation,
40 are thought to produce sheet-like sand bodies, whereas limited translation and significant
41 aggradation of submarine-channel bends result in stacks of ribbon-like sand bodies (Peakall et al.,
42 2000). Early work on submarine-channel evolution has suggested that downstream translation is
43 rare or nonexistent (e.g., Peakall et al., 2000). However, downstream translation has been observed
44 since then in three-dimensional (3D) seismic-reflection datasets and sometimes attributed to
45 allogenic changes in sediment delivery to the system (e.g., Posamentier, 2003; Posamentier and
46 Kolla, 2003; Kolla et al., 2012; Janocko et al., 2013). Although channel migration is often

47 discussed in terms of expansion, translation, and rotation, a clear understanding of when and why
48 channel bends expand or translate is still lacking. This is especially true for submarine channels.

49 Based on insights from rivers (Howard and Knutson, 1984; Smith et al., 2009; Ghinassi et
50 al., 2016), we propose that downstream translation of bends might be common in settings that
51 promote the generation of high-curvature bends, either as a result of cutoffs or other perturbations
52 to the equilibrium plan-view channel pattern. Such settings include deep-water salt-tectonic
53 provinces (Hudec and Jackson, 2007), in which rapid rates of deformation commonly create
54 complex topography that localizes channel pathways and depocenters (e.g., Gee and Gawthorpe,
55 2008). Channel-sculpting sediment-gravity flows tend to follow the direction of steepest descent
56 across a slope, and salt deformation can create topography that draws gravity flows away from the
57 regional slope of a continental margin. The resulting sediment-dispersal system might contain
58 complex and surprising channelized stratigraphic patterns, such as anomalous meander-loop
59 geometries (e.g., Mendoza-Veloza, 2007). Notably, these stratigraphic patterns are a result of
60 tectonic deformation and gravity-flow interactions with the resultant topography, independent of
61 any major changes in sediment delivery to the submarine-channel system.

62 Here, we use 3D seismic-reflection data from the Campos basin, offshore Brazil, to
63 characterize the structural geometry of a salt diapir and stratigraphic architecture of a ~18 km-long
64 reach of a submarine-channel system (Figs. 1, 2). We interpret the structural and stratigraphic
65 evolution, including meander-cutoff development adjacent to a salt diapir followed by ~10 km of
66 downstream translation of a channel bend. We test the stratigraphic evolution with a simple
67 numerical model that we have developed based on the Howard and Knutson (1984) meandering-
68 channel model (Sylvester and Covault, 2016). Our goal with this subsurface characterization and
69 stratigraphic modeling study is to shed light on the processes and controls of submarine-channel

70 downstream translation, which might be common in rapidly deforming settings, like salt basins,
71 that promote localized subsidence, meander cutoffs, and rapidly translating, high-curvature bends.

72

73 **GEOLOGIC SETTING**

74 The Campos basin is located in water depths >200 m along the southeastern continental
75 margin of Brazil in the South Atlantic Ocean (Carminatti and Scarton, 1991; Bruhn et al., 2003)
76 (Fig. 1). It is separated from the adjacent Espirito Santo (to the north) and Santos (to the south)
77 basins by northwest-southeast-oriented basement highs (Guardado et al., 2000). The Campos basin
78 is one of the most productive hydrocarbon-bearing basins in the world (Mohriak et al., 1990); in
79 2017, total daily production was 1.3 million barrels of oil and 25 million cubic meters of natural
80 gas from a variety of reservoirs, including Cretaceous to Miocene siliciclastic turbidites (Mohriak
81 et al., 1990; Bruhn et al., 2003).

82 The Campos basin initiated during Late Jurassic breakup of Gondwana and opening of the
83 South Atlantic Ocean (Guardado et al., 1990). The basin fill comprises Berriasian-early Aptian
84 continental rift deposits, overlain by middle Aptian salt, an early-middle Albian carbonate
85 platform, and a late Albian to present succession of progressively deeper-water continental-margin
86 deposits (Bruhn, 1998). The Cretaceous-present paleoflow direction is generally northwest-to-
87 southeast because of the regional slope of the Brazilian continental margin (Fig. 1). However,
88 paleoflow direction in the Campos basin varies depending on local structural configuration and
89 orientation of topographic lows; in an MS thesis at the University of Texas at Austin, Ceyhan
90 (2017) interpreted northwest-to-southeast, west-to-east, and north-to-south paleoflow for
91 Pliocene-Pleistocene channel systems.

92 The Aptian salt plays an important role in establishing the structural style of the Campos
93 basin. The base of the Aptian is a detachment surface (Fetter, 2009). Below the detachment, the
94 main structural features are horsts and grabens bounded by steep normal faults active during Early
95 Cretaceous rifting (Chang et al., 1992). Above the detachment, salt deformation was initiated by
96 early Albian eastward basin tilting (De Gasperi and Catuneanu, 2014). Salt deformation has
97 resulted in structural domains including a proximal domain of east-to-west extension and
98 extensional diapirs, an extensional to compressional intermediate, transitional domain of west-to-
99 east translation and shortened diapirs, and a distal domain of west-to-east contraction within a fold-
100 and-thrust belt (Demercian et al., 1993; Mohriak et al., 2012). We focused on the seismic
101 stratigraphy of a Miocene submarine-channel system in the intermediate structural domain of the
102 Campos basin (Fig. 1).

103

104 **DATA AND METHODS**

105 **Subsurface data and interpretation**

106 We used amplitude and coherence (i.e., similarity between adjacent seismic traces;
107 Bahorich and Farmer, 1995) attributes generated from a Kirchhoff pre-stack depth-migrated 3D
108 seismic-reflection volume with wavelengths at the depths of interest of ~20-50 m (vertical
109 resolution ~5-12.5 m) and 25 m horizontal sampling rate. The seismic-reflection volume was
110 donated by Investigaç o Petrol fera Limitada (PGS). Seismic-reflection data were processed to
111 zero phase. We used the Paradigm® SeisEarth® interpretation and visualization product suite to
112 map six regional horizons based on line-by-line continuity and terminations of relatively high-
113 amplitude seismic reflections (Figs. 2, 3). We used root mean square (RMS) amplitude maps to
114 highlight channel systems to interpret in more detail (cf. De Ruig and Hubbard, 2006) (Fig. 4). We

115 also interpreted a series of discontinuous, high-amplitude seismic reflections defining channelized
116 deposits by selecting a reflection and using a 3D propagator algorithm to cross-correlate nearest-
117 neighbor seismic traces to within a defined confidence interval (Fig. 5) (cf. Madof et al., 2009).
118 Horizons 1 and 6 are interpreted to be base and top, respectively, of the Miocene based on Ceyhan
119 (2017) and published seismic-stratigraphic studies and stratigraphic charts (Winter et al., 2007;
120 Fetter, 2009; Contreras et al., 2010; Contreras, 2011).

121 We used Midland Valley's Move® software to apply 2D restoration to the cross-section
122 profile A of Figure 3. For the restored sections, we assumed a regional topographic slope of 0.18° ,
123 which is parallel to the modern slope in the study area. We interpreted deflections to this regional
124 slope based on the positions of channel systems, which we assumed to follow topographic lows.
125 We restored all bedding to the topographic surface using flexural slip because we interpreted that
126 salt diapir uplift was a result of regional shortening (see below). We did not decompact sediment
127 because our primary concern in the restorations was the evolution of surface topography.
128 Therefore, unit thicknesses are incorrect, but we have captured the interplay between salt
129 deformation and topography.

130

131 **Numerical model of channel evolution**

132 We employ a simple kinematic meandering model that is based on Howard and Knutson
133 (1984), using a formulation that is equivalent to the approach of Ikeda et al. (1981) (Sun et al.,
134 1996), to better understand the migration patterns of submarine channels (i.e., expansion and
135 translation). A key aspect of this model is that migration rate is a function of the weighted sum of
136 upstream curvatures. To compute the migration rate, the upstream curvatures are converted to a
137 “nominal” migration rate, defined as follows:

138

$$R_0 = \frac{k_l W}{R} (1)$$

139

where R_0 is the nominal migration rate, k_l is a migration rate constant, W is channel width, and R

140

is radius of curvature. Then, the actual migration rate R_1 can be estimated using:

141

$$R_1(s) = \Omega R_0(s) + (\Gamma \int_0^\infty R_0(s - \xi) G(\xi) d\xi) (\int_0^\infty G(\xi) d\xi)^{-1} (2)$$

142

where Ω and Γ are weighting parameters with values of -1 and 2.5, and $G(\xi)$ is an exponential

143

weighting function:

144

$$G(\xi) = e^{-\alpha \xi} (3)$$

145

The weighting decreases exponentially with distance ξ from the point of interest and the

146

exponent α is a function of channel depth D and the friction factor C_f ,

147

$$\alpha = 2k \frac{C_f}{D} (4)$$

148

where k is a constant that takes the value of 1.0 (Howard and Knutson, 1984). In the original

149

formulation of the model, in an attempt to mimic the observations of Hickin and Nanson (1975),

150

curvatures higher than a critical value result in a lower migration rate (Howard and Knutson, 1984).

151

However, new data from modern rivers suggest that migration rate increases with higher

152

curvatures (Furbish, 1988; Sylvester et al., in revision); therefore, for all curvature values, we use

153

a simple linear relationship between curvature and nominal migration rate (Eq. 1).

154

The Howard and Knutson (1984) model has been previously used in modeling subaerial

155

and submarine meander development (e.g., Finnegan and Dietrich, 2011; Limaye and Lamb, 2014;

156

Sylvester and Covault, 2016). While the model we are using only captures the large-scale

157

kinematics of meandering and does not reproduce phenomena like compound meander

158

development and upstream influence of curvature, it captures well the translation and expansion

159

of meander bends and it provides a simple framework with a small number of parameters to explore

160

the origins of the unusual bends observed in the Campos basin.

161

162 **RESULTS**

163 **Subsurface characterization**

164 We mapped six horizons across a ~12 x 18 km area of the intermediate, transitional
165 structural domain of the Campos basin, in water depths between ~2100-2500 m (Fig. 1). We will
166 describe the seismic character from the base of the subsurface section (horizon 1) to the top
167 (horizon 6) (Figs. 2, 3). We did not interpret the detailed seismic-stratigraphic architecture between
168 horizons 1 and 3; we mapped these horizons for the purposes of the structural restoration presented
169 below (Fig. 7).

170 Horizon 1 is the base of a section of seismic reflections including a high-amplitude package
171 confined within large-scale concave-up surfaces defined by reflection terminations (Figs 2, 3).
172 Reflections are more continuous and lower amplitude outside of the concave-up surfaces (Fig. 3).
173 An RMS-amplitude extraction between horizons 1 and 2 shows a north-south-oriented channel
174 pattern, which is continuous across a salt diapir (Fig. 4A). Seismic reflections are truncated against
175 the western side of the diapir (Fig. 3). We interpret that the package of high-amplitude seismic
176 reflections between horizons 1 and 2 represents channel deposits. The trend of the channel system
177 is oriented directly over the salt diapir (Fig. 4A); therefore, the channel system likely initiated
178 while there was no positive relief over the salt diapir (Fig. 6B). Overlying this channel system,
179 seismic reflections onlap horizon 2 and are truncated by horizon 3 (Fig. 3).

180 Horizon 3 defines a ~2 km wide and straight, north-south-oriented erosional surface (Fig.
181 2). In the northeast of the study area, the erosional surface is truncated by the salt diapir, and
182 includes an arcuate scour to the west of the diapir (Fig. 2). High-amplitude, discontinuous seismic
183 reflections are confined by the erosional surface (see RMS-amplitude extraction between horizons
184 3 and 5; Fig. 4B), with a thin section of more continuous reflections outside of it (Fig. 3). We

185 interpret that horizon 3 defines the base of another channel system. Horizons 4 and 5 define the
186 base and top, respectively, of a relatively narrow (< 1 km) channel form (Figs. 2, 3). This channel
187 form is the last-active channel of the system. Overlying horizon 5 is a section of low-to-moderate
188 amplitude, chaotic seismic reflections that we interpret to be mass-transport deposits (Fig. 3).
189 These deposits are emplaced from northwest to southeast (Figs. 2, 3). The channel system appears
190 to shutdown with the emplacement of mass-transport deposits overlying horizon 5. Horizon 6
191 locally truncates horizons 3, 4, and 5 (Figs. 2, 3) and forms the base of a sequence of Pliocene-
192 Pleistocene channel and mass-transport deposits, which were studied by Ceyhan (2017). The
193 channel system between horizons 3 and 5 exhibits the characteristics of meander cutoff and
194 downstream translation in a topographic low adjacent to a salt diapir and is the main focus of this
195 study (Figs. 5, 6A). Below we will provide more detailed interpretations of the seismic-
196 stratigraphic architecture of this channel system.

197 A coherence attribute map between horizons 3 and 5 shows a pair of channel-bend cutoffs
198 in a syncline adjacent to the northeastern diapir (Fig. 5). These cutoffs are truncated by the last-
199 active channel defined by horizons 4 and 5, which exhibits a pair of $\sim 90^\circ$ bends as it crosses the
200 diapir (Fig. 5). This last-active channel is approximately straight as it descends to the south, where
201 it exhibits another pair of sharp bends. Upstream from these bends, low coherence values define
202 arcuate shapes, which are parallel to the concave (outer) bend of the last channel (Fig. 5). These
203 arcuate shapes are defined by north-to-south dipping, downstream-translating, high-amplitude
204 seismic reflections in cross section (Fig. 5b). This stratigraphic architecture suggests a channel
205 evolution beginning with the development of highly sinuous meanders in a syncline adjacent to
206 salt, followed by cutoff and the generation of a high-curvature perturbation, which resulted in
207 multiple bends that translated ~ 10 km downstream from north to south. Remnant channel deposits

208 with concave bends, parallel to the outer bend of the last channel, developed in the wake of this
209 downstream translation. We have two remaining questions. First, is this channel evolution
210 feasible? Our interpretation of the seismic-stratigraphic architecture and evolution of the channel
211 system between horizons 3 and 5 is a hypothesis to test with a simple forward model of
212 meandering-channel evolution (Sylvester and Covault, 2016). Second, if the seismic-stratigraphic
213 evolution is confirmed by numerical modeling, what is the underlying control on the sequence of
214 meander-loop expansion, cutoff, and downstream translation? Specifically, what is the role of
215 structural deformation in promoting these processes in tectonically active salt basins? Some of the
216 key channelized stratigraphic patterns in the study area are associated with the northeastern diapir;
217 to understand the growth of this diapir and the resultant topography, we apply a 2D structural
218 restoration to the cross-section profile A of Figure 3.

219

220 **Structural restoration**

221 Based on the observation that the channel system passed directly over the salt diapir (Fig.
222 4A), we conclude that the diapir had little or no positive relief between deposition of horizons 1
223 and 2 (Fig. 6B). Deposits between horizons 2 and 5, however, thin dramatically onto the diapir.
224 Furthermore, horizon 5 incises the diapir roof. These observations suggest that renewed uplift of
225 the diapir started after horizon 2. What could have caused this? We interpret a mild shortening
226 event beginning at horizon 2 time; the unit between horizons 1 and 2 is nearly isopachous on the
227 east side of the diapir, and it is then uplifted, onlapped, and truncated (see profile A of Fig. 3).
228 Uplift of an isopachous roof is a diagnostic feature of diapir shortening (e.g., Vendeville and
229 Nilsen, 1995).

230 We constructed our section restoration using this contractional interpretation (Fig. 7). We
231 interpreted a slight topographic low above the diapir, possibly as a result of salt dissolution, prior
232 to the onset of shortening. This topographic low focused a channel system over the diapir crest
233 (see ‘horizon 2 – pre shortening’ of Fig. 7). Mild shortening arched and uplifted the diapir crest.
234 Uplift above and adjacent to the diapir created a syncline to the west of the diapir, at the intersection
235 of the east-dipping regional slope and the west-dipping flank of the diapir uplift (see ‘horizon 2 –
236 post shortening’ of Fig. 7). The supradiapir channel system shifted to this syncline, where it cut
237 the meander loops at horizon 3 (see ‘horizon 3’ structure map of Fig. 2). These meanders are at
238 the base of the channel-bend cutoffs between horizons 3 and 5. Shortening continued to the present
239 based on folding of younger units and erosion of the modern seafloor (Fig. 7). Total shortening in
240 the restoration is only 85 m; however, even this modest shortening was sufficient to change
241 seafloor topography and shift channel-system location.

242

243 **Numerical model of channel evolution**

244 Most numerical models of meandering are initialized with a straight centerline that has
245 random noise added throughout its entire length (e.g., Sun et al., 1996; Limaye and Lamb, 2013).
246 Although both expansion and translation are common in these models, long stretches of deposits
247 showing downstream translation are rarely preserved, as their upstream side gets rapidly eroded
248 by the upstream meanders. The seismic-reflection data show highly sinuous channel cutoffs in a
249 syncline adjacent to a salt diapir, which transition downstream to a straighter channel with a few
250 bends downstream of the structure (Fig. 5). In general, for simple geometric reasons, cutoff events
251 result in small but high-curvature bends (e.g., Camporeale et al., 2008). Therefore, we have used
252 an initial condition with a single perturbation of relatively high curvature that affects an otherwise

253 straight channel (Figs. 8, 9 and Supplementary Animations 1, 2). It is tempting to think that for a
254 given channel size, the amount of translation and expansion would be the same. However, the
255 duration and length of translation are affected by channel depth D and friction factor C_f of the
256 exponent α (Eq. 4). In general, a smaller value of α results in longer downstream translation (Fig.
257 8 and Supplementary Animation 1). To generate translation similar to that observed in the Campos
258 basin example, we applied a relatively small width-to-depth ratio and a small friction factor. We
259 found that values of $W= 300$ m, $D= 30$ m, and $C_f= 0.01275$ result in a reasonable match to the
260 channel system in the Campos basin (Fig. 9 and Supplementary Animation 2). These depth and
261 width values are likely to be representative of the lower, higher density part of the channel-
262 sculpting sediment-gravity flows, which probably drive the evolution of the plan-view pattern and
263 the width-to-wavelength scaling (cf. Pirmez and Imran, 2003). Of course, larger values of D give
264 the same result if C_f is increased by the same amount. The initial bend migrates downstream,
265 leaving behind deposits; at the same time, two or three additional bends develop further
266 downstream, in a wave-like fashion (Fig. 9 and Supplementary Animation 2). These bends are
267 strongly translational in nature and leave behind significant translation-related deposits similar in
268 scale to the channel deposits in the Campos basin. However, the preservation potential of these
269 deposits is variable: as bends gradually switch from translation to expansion, the translation-related
270 units of the downstream bends tend to be eroded, and only the downstream migration of the first
271 couple of bends is preserved (e.g., see model with $\alpha = 0.0015$ of Fig. 8 and Supplementary
272 Animation 1). The Campos basin example we have described here is likely a relatively short-lived
273 feature that has developed from a low-sinuosity, newly established channel with a single
274 perturbation and was abandoned before meander expansion took over from translation. Indeed, the

275 channel system is shutdown following the emplacement of the mass-transport complex above
276 horizon 5.

277

278 **DISCUSSION**

279 Our numerical model results are similar to the seismic-reflection example from the Campos
280 basin: upstream meander cutoffs result in a high-curvature perturbation that initiates additional
281 bends downstream, and all bends leave downstream-translating channel deposits in their wake
282 (Figs. 5, 9). The geomorphologic and stratigraphic expression of these deposits is reminiscent of
283 fluvial counter-point bars (Fig. 9C). Counter-point bars form where long-term deposition takes
284 place on a concave bank; the corresponding deposits are usually finer grained than those of the
285 point bar (Smith et al., 2009). Qualitatively, counter-point bars have been linked to downstream
286 translation and confinement; although there is evidence that confinement is not always necessary.
287 Sharp and small cutoff-related bends in rivers often result in significant translation and are likely
288 locations of counter-point bar formation (Fig. 9C).

289 Our integrated seismic-stratigraphic interpretation and numerical modeling suggests that
290 translation might be common in settings that promote (1) meander cutoffs and the generation of
291 high-curvature bends, and (2) repeated local re-establishment of relatively straight channels. The
292 former can happen in salt-tectonic provinces, in which deformation can draw channel pathways
293 into low topography (e.g., Gee and Gawthorpe, 2006; Oluboyo et al., 2014). The latter can happen
294 when a large mass-transport event erases the existing channel topography, either through erosion
295 or burial, and sets the stage for a new channel with low sinuosity. These conditions are satisfied
296 by continental margins affected by salt tectonics, such as the area of this study in the Campos
297 basin. Here, a syncline adjacent to a salt diapir appears to have localized sinuous meander loops,

298 which were cut off as they expanded into the syncline. Other examples of downstream translation
299 of submarine-channel bends have been linked to major changes in flow regime and type of
300 sediment load. However, we propose that allogenic changes in sediment delivery to the system are
301 not necessary to produce these deposits and downstream translation might be common in rapidly
302 deforming settings, like salt basins, that promote localized subsidence, meander cutoffs, and
303 rapidly translating, high-curvature bends.

304 With respect to the architecture of continental margins, submarine-channel systems
305 commonly include a complex stacking of erosional remnants of sandstone-dominated channel fills
306 (Deptuck et al., 2003; 2007; Hodgson et al., 2011; McHargue et al., 2011; Sylvester et al., 2011),
307 especially during their early evolution when cutoffs are more common (Sylvester and Covault,
308 2016). This architecture is reminiscent of the sheet-like sand bodies produced by the combined
309 translation and expansion of rivers, although aggradation is often significantly higher in submarine
310 channels (Jobe et al., 2016). Further work is needed to evaluate whether (1) downstream translation
311 is more common in submarine channels than in rivers and (2) submarine “counter-point bars” are
312 relatively fine-grained, like in rivers (Smith et al. 2009). Our results and observations suggest that
313 long-term and long-distance translation is an important component of submarine-channel
314 evolution, and, similar to rivers, it is primarily driven by the downstream shift of the location of
315 maximum migration relative to the bend apex (Furbish, 1988; Sylvester et al., in revision). This
316 phase lag is well known from meandering models (e.g., Seminara, 2006) and is the result of the
317 influence of upstream curvatures on the local migration rate. This influence and the resulting
318 translation are stronger when the channel is deep and friction factor is low (e.g., a smaller value of
319 α ; Fig. 8 and Supplementary Animation 1); therefore, a possible explanation for the excessive
320 translation observed in the Campos basin and elsewhere is that submarine channels tend to be

321 overall deeper and, perhaps due to the lack of large mid-channel bars and bedforms, smoother than
322 their fluvial counterparts.

323

324 **CONCLUSIONS**

325 We characterized the structural and seismic-stratigraphic evolution of a Miocene salt diapir
326 and submarine-channel system in the tectonically active Campos salt basin. Structural restoration
327 shows diapir shortening created a syncline to the west of the diapir, which localized a channel-
328 system depocenter comprising meander cutoffs (Fig. 7). We used a simple forward model of
329 meandering-channel evolution to show that these upstream meander cutoffs resulted in a high-
330 curvature perturbation that initiated additional bends downstream, and all bends left downstream-
331 translating channel deposits in their wake (Fig. 9 and Supplementary Animation 2). These deposits
332 are reminiscent of fluvial counter-point bars, which might commonly develop during the early
333 evolution of relatively deep, smooth-floored submarine-channel systems, and, in general, after the
334 formation of high-curvature perturbations. Moreover, we show that downstream translation can
335 develop without allogenic changes in sediment delivery to the system and without any
336 confinement. Early work on submarine-channel evolution has suggested that downstream
337 translation is rare; we suspect it to be a common migration process in submarine-channel systems
338 in salt basins and other tectonically active settings with complex topography, which might promote
339 the development of cutoffs and other perturbations.

340

341 **ACKNOWLEDGMENTS**

342 We thank Investigação Petrolífera Limitada (PGS) for the donation of seismic-reflection data. We
343 are grateful to Emerson for the donation of Paradigm SeisEarth® interpretation and visualization
344 software. We thank the sponsors of the Quantitative Clastics Laboratory
345 (<http://www.beg.utexas.edu/qcl>) and the Applied Geodynamics Laboratory
346 (<http://www.beg.utexas.edu/agl>). We acknowledge former AGL researcher Dan Carruthers for
347 initiating chronostratigraphic analysis of the data in the Campos basin. We thank Oliver Duffy and
348 Naiara Fernandez for early assistance with the structural deformation of the Campos basin. We are
349 grateful to Paul Durkin and David Mohrig for discussions about channel-bend translation and
350 counter-point bars.

351

352 **REFERENCES CITED**

353 Bahorich, M. S., and Farmer, S. L., 1995, 3-D seismic discontinuity for faults and stratigraphic
354 features; The coherence cube: SEG Technical Program Expanded Abstracts 1995, Society
355 of Exploration Geophysicists, p. 93-96.

356 Barnes, N. E., and Normark, W. R., 1985, Diagnostic parameters for comparing modern submarine
357 fans and ancient turbidite systems, in Bouma, A. H., Normark, W. R., and Barnes, N. E.,
358 eds., Submarine fans and related turbidite systems: Springer, New York, NY, p. 13-14.

359 Bruhn, C. H. L., 1998, Major types of deep-water reservoirs from the eastern Brazilian rift and
360 passive margin basins: AAPG International Conference & Exhibition, Rio de Janeiro,
361 Brazil, AAPG Search and Discovery Article #90933.

362 Bruhn, C. H., Gomes, J. A. T., Del Lucchese Jr, C., and Johann, P. R., 2003, Campos basin;
363 Reservoir characterization and management-Historical overview and future challenges:
364 Offshore Technology Conference, Houston, Texas, OTC-15220-MS.

365 Camporeale, C., Perucca, E., and Ridolfi, L., 2008, Significance of cutoff in meandering river
366 dynamics: *Journal of Geophysical Research Earth Surface*, 113(F1).

367 Carminatti, M., and Scarton, J. C., 1991, Sequence stratigraphy of the Oligocene turbidite complex
368 of the Campos Basin, offshore Brazil; an overview: in Weimer, P., and Link, M. H., eds.,
369 Seismic facies and sedimentary processes of submarine fans and turbidite systems:
370 Springer, New York, NY, 241-246.

371 Ceyhan, C., 2017, Interplay of salt-influenced structural deformation and submarine channel
372 evolution in the Campos Basin, offshore Brazil [M. S. thesis]: the University of Texas at
373 Austin, 80 p.

374 Chang, H. K., Kowsmann, R. O., Figueiredo, A. M. F., and Bender, A., 1992, Tectonics and
375 stratigraphy of the East Brazil Rift system; an overview: *Tectonophysics*, v. 213, p. 97-
376 138.

377 Contreras, J., 2011, Seismo-stratigraphy and numerical basin modeling of the southern Brazilian
378 continental margin (Campos, Santos, and Pelotas basins) [Ph. D. thesis]: Ruprecht-Karls-
379 Universität, Heidelberg, Germany, 146 p.

380 Contreras, J., Zühlke, R., Bowman, S., and Bechstädt, T., 2010, Seismic stratigraphy and
381 subsidence analysis of the southern Brazilian margin (Campos, Santos and Pelotas basins):
382 *Marine and Petroleum Geology*, v. 27, p. 1952-1980.

383 Damuth, J. E., Kolla, V., Flood, R. D., Kowsmann, R. O., Monteiro, M. C., Gorini, M. A., Palma,
384 J. J. C., and Belderson, R. H., 1983, Distributary channel meandering and bifurcation

385 patterns on the Amazon deep-sea fan as revealed by long-range side-scan sonar (GLORIA):
386 Geology, v. 11, p. 94-98.

387 De Gasperi, A., and Catuneanu, O., 2014, Sequence stratigraphy of the Eocene turbidite reservoirs
388 in Albacora field, Campos Basin, offshore Brazil: AAPG bulletin, v. 98, p. 279-313.

389 Demercian, S., Szatmari, P., and Cobbold, P. R., 1993, Style and pattern of salt diapirs due to thin-
390 skinned gravitational gliding, Campos and Santos basins, offshore Brazil: Tectonophysics,
391 v. 228, p. 393-433.

392 Deptuck, M. E., Steffens, G. S., Barton, M., and Pirmez, C., 2003, Architecture and evolution of
393 upper fan channel-belts on the Niger Delta slope and in the Arabian Sea: Marine and
394 Petroleum Geology, v. 20, p. 649-676.

395 Deptuck, M. E., Sylvester, Z., Pirmez, C., and O'Byrne, C., 2007, Migration–aggradation history
396 and 3-D seismic geomorphology of submarine channels in the Pleistocene Benin-major
397 Canyon, western Niger Delta slope: Marine and Petroleum Geology, v. 24, p. 406-433.

398 De Ruig, M. J., and Hubbard, S. M., 2006, Seismic facies and reservoir characteristics of a deep-
399 marine channel belt in the Molasse foreland basin, Puchkirchen Formation, Austria: AAPG
400 bulletin, v. 90, p. 735-752.

401 Fetter, M., 2009, The role of basement tectonic reactivation on the structural evolution of Campos
402 Basin, offshore Brazil; Evidence from 3D seismic analysis and section restoration: Marine
403 and Petroleum Geology, v. 26, p. 873-886.

404 Finnegan, N. J., and Dietrich, W. E., 2011, Episodic bedrock strath terrace formation due to
405 meander migration and cutoff: Geology, v. 39, p. 143-146.

406 Furbish, D. J., 1988, River-bend curvature and migration; How are they related?: Geology, v. 16,
407 p. 752-755.

408 Galy, V., Beyssac, O., France-Lanord, C., and Eglinton, T., 2008, Recycling of graphite during
409 Himalayan erosion; a geological stabilization of carbon in the crust: *Science*, v. 322, p.
410 943-945.

411 Gee, M. J. R., and Gawthorpe, R. L., 2006, Submarine channels controlled by salt tectonics;
412 Examples from 3D seismic data offshore Angola: *Marine and Petroleum Geology*, v. 23,
413 p. 443-458.

414 Ghinassi, M., Ielpi, A., Aldinucci, M., and Fustic, M., 2016, Downstream-migrating fluvial point
415 bars in the rock record: *Sedimentary Geology*, v. 334, p. 66-96.

416 Gorelick, N., Hancher, M., Dixon, M., Ilyushchenko, S., Thau, D., and Moore, R., 2017, Google
417 Earth Engine; Planetary-scale geospatial analysis for everyone: *Remote Sensing of*
418 *Environment*, v. 202, p. 18-27.

419 Guardado, L. R., Gamboa, L. A. P., and Lucchesi, C. F., 1990, Petroleum geology of the Campos
420 Basin, Brazil, a model for a producing Atlantic type basin: *AAPG memoir*, v. 48, p. 3-36.

421 Guardado, L. R., Spadini, A. R., Brandão, J. S. L., and Mello, M. R., 2000, Petroleum system of
422 the Campos Basin, Brazil: *AAPG memoir*, v. 73, p. 317-324.

423 Hickin, E. J., and Nanson, G. C., 1975, The character of channel migration on the Beatton River,
424 northeast British Columbia, Canada: *Geological Society of America Bulletin*, v. 86, p. 487-
425 494.

426 Hodgson, D. M., Di Celma, C. N., Brunt, R. L., and Flint, S. S., 2011, Submarine slope degradation
427 and aggradation and the stratigraphic evolution of channel–levee systems: *Journal of the*
428 *Geological Society*, v. 168, p. 625-628.

429 Howard, A. D., and Knutson, T. R., 1984, Sufficient conditions for river meandering; A simulation
430 approach: *Water Resources Research*, v. 20, p. 1659-1667.

431 Hubbard, S. M., Covault, J. A., Fildani, A., and Romans, B. W., 2014, Sediment transfer and
432 deposition in slope channels; Deciphering the record of enigmatic deep-sea processes from
433 outcrop: Geological Society of America Bulletin, v. 126, p. 857-871.

434 Hudec, M. R., and Jackson, M. P., 2007, Terra infirma; Understanding salt tectonics: Earth-
435 Science Reviews, v. 82, p. 1-28.

436 Ikeda, S., Parker, G., and Sawai, K., 1981, Bend theory of river meanders. Part 1. Linear
437 development: Journal of Fluid Mechanics, v. 112, p. 363-377.

438 Janocko, M., Nemeč, W., Henriksen, S., and Warchoł, M., 2013, The diversity of deep-water
439 sinuous channel belts and slope valley-fill complexes: Marine and Petroleum Geology, v.
440 41, p. 7-34.

441 Jobe, Z. R., Howes, N. C., and Auchter, N. C., 2016, Comparing submarine and fluvial channel
442 kinematics: Implications for stratigraphic architecture: Geology, v. 44, p. 931-934.

443 Kolla, V., Bandyopadhyay, A., Gupta, P., Mukherjee, B., and Ramana, D. V., 2012, Morphology
444 and internal structure of a recent upper Bengal fan-valley complex, in Prather, B. E.,
445 Deptuck, M. E., Mohrig, D., von Hoorn, B., and Wynn, R. B., Application of the Principles
446 of Seismic Geomorphology to Continental-Slope and Base-of-Slope Systems; Case Studies
447 from Seafloor and Near-Seafloor Analogues: SEPM Special Publication, v. 99, p. 347-369.

448 Limaye, A. B., and Lamb, M. P., 2014, Numerical simulations of bedrock valley evolution by
449 meandering rivers with variable bank material: Journal of Geophysical Research Earth
450 Surface, v. 119, p. 927-950.

451 Madof, A. S., Christie-Blick, N., and Anders, M. H., 2009, Stratigraphic controls on a salt-
452 withdrawal intraslope minibasin, north-central Green Canyon, Gulf of Mexico;
453 Implications for misinterpreting sea level change: AAPG bulletin, v. 93, p. 535-561.

454 McHargue, T., Pyrcz, M. J., Sullivan, M. D., Clark, J. D., Fildani, A., Romans, B. W., Covault, J.
455 A., Levy, M., Posamentier, H. W., and Drinkwater, N. J., 2011, Architecture of turbidite
456 channel systems on the continental slope; Patterns and predictions: Marine and Petroleum
457 Geology, v. 28, p. 728-743.

458 Mendoza-Veloza, R., 2007, The architecture of lower-slope channel complexes, offshore Gabon,
459 West Africa [M. S. thesis]: the University of Texas at Austin, 110 p.

460 Mohriak, W. U., Mello, M. R., Dewey, J. F., and Maxwell, J. R., 1990, Petroleum geology of the
461 Campos Basin, offshore Brazil: Geological Society, London, Special Publications, v. 50,
462 p. 119-141.

463 Mohriak, W. U., Szatmari, P., and Anjos, S., 2012, Salt; Geology and tectonics of selected
464 Brazilian basins in their global context: Geological Society, London, Special Publications,
465 v. 363, p. 131-158.

466 Oluboyo, A. P., Gawthorpe, R. L., Bakke, K., and Hadler-Jacobsen, F., 2014, Salt tectonic controls
467 on deep-water turbidite depositional systems; Miocene, southwestern Lower Congo Basin,
468 offshore Angola: Basin Research, v. 26, p. 597-620.

469 Peakall, J., McCaffrey, B., and Kneller, B., 2000, A process model for the evolution, morphology,
470 and architecture of sinuous submarine channels: Journal of Sedimentary Research, v. 70,
471 p. 434-448.

472 Peres, W. E., 1993, Shelf-fed turbidite system model and its application to the Oligocene deposits
473 of the Campos Basin, Brazil: AAPG bulletin, v. 77, p. 81-101.

474 Pettingill, H. S., and Weimer, P., 2002, Worldwide deepwater exploration and production; Past,
475 present, and future: The Leading Edge, v. 21, p. 371-376.

476 Piper, D. J., and Normark, W. R., 2001, Sandy fans-from Amazon to Hueneme and beyond: AAPG
477 bulletin, v. 85, p. 1407-1438.

478 Pirmez, C., and Imran, J., 2003, Reconstruction of turbidity currents in Amazon Channel: Marine
479 and Petroleum Geology, v. 20, p. 823-849.

480 Posamentier, H. W., 2003, Depositional elements associated with a basin floor channel-levee
481 system: case study from the Gulf of Mexico: Marine and Petroleum Geology, v. 20, p. 677-
482 690.

483 Posamentier, H. W., and Kolla, V., 2003, Seismic geomorphology and stratigraphy of depositional
484 elements in deep-water settings: Journal of Sedimentary Research, v. 73, p. 367-388.

485 Romans, B. W., Castellort, S., Covault, J. A., Fildani, A., and Walsh, J. P., 2016, Environmental
486 signal propagation in sedimentary systems across timescales: Earth-Science Reviews, v.
487 153, p. 7-29.

488 Seminara, G., 2006, Meanders: Journal of Fluid Mechanics, v. 554, p. 271-297.

489 Smith, D. G., Hubbard, S. M., Leckie, D. A., and Fustic, M., 2009, Counter point bar deposits;
490 Lithofacies and reservoir significance in the meandering modern Peace River and ancient
491 McMurray Formation, Alberta, Canada: Sedimentology, v. 56, p. 1655-1669.

492 Sun, T., Meakin, P., Jøssang, T., and Schwarz, K., 1996, A simulation model for meandering
493 rivers: Water Resources Research, v. 32, p. 2937-2954.

494 Sylvester, Z., and Covault, J. A., 2016, Development of cutoff-related knickpoints during early
495 evolution of submarine channels: Geology, v. 44, p. 835-838.

496 Sylvester, Z., Covault, J., and Durkin, P., in revision, High curvatures drive river meandering:
497 Geology.

498 Sylvester, Z., Pirmez, C., and Cantelli, A., 2011, A model of submarine channel-levee evolution
499 based on channel trajectories; Implications for stratigraphic architecture: *Marine and*
500 *Petroleum Geology*, v. 28, p. 716-727.

501 Vendeville, B. C., and Nilsen, K. T., 1995, Episodic growth of salt diapirs driven by horizontal
502 shortening: *SEPM Gulf Coast Section 16th Annual Research Foundation Conference*, v.
503 285, p. 295.

504 Winter, W. R., Jahnert, R. J., and França, A. B., 2007, Bacia de campos: *Boletim de Geociencias*
505 *da Petrobras*, v. 15, p. 511-529.

506 Wynn, R. B., Cronin, B. T., and Peakall, J., 2007, Sinuous deep-water channels; Genesis, geometry
507 and architecture: *Marine and Petroleum Geology*, v. 24, p. 341-387.

508

509 **FIGURE CAPTIONS**

510 Figure 1. (A) Study area in the deep-water Campos basin. Gray polygon indicates location of
511 seismic-reflection volume in B. Modified from Peres (1993). (B) Seafloor of the study area.
512 Black dashed rectangle indicates location of maps in Figure 2.

513 Figure 2. (Above) Structure maps of horizons 1-6. Horizontal white lines in horizon 2 map indicate
514 locations of west-east profiles in Figure 3. (Below) Isochore maps between horizons.

515 Figure 3. West-east seismic-reflection profiles (left) and interpreted depositional elements (right).
516 Profiles are oriented west (left) to east (right). Profile locations are in Figure 2. Black
517 dashed rectangles in seismic-reflection profiles (left) indicate locations of interpreted
518 depositional elements (right).

519 Figure 4. RMS-amplitude maps between horizons 1-2 (A) and horizons 3-5 (B).

520 Figure 5. Detailed seismic-stratigraphic interpretation of channel system between horizons 3-5.
521 (Above) Uninterpreted (left) and interpreted (right) coherence maps. Solid black lines in
522 interpreted (right) coherence map indicate locations of seismic-reflection profiles below.
523 (Below) Interpreted seismic-reflection profile b-b' shows a depositional-dip view of north-
524 to-south dipping, downstream-translating, high-amplitude seismic reflections. Profile c-c'
525 shows a depositional-strike view of the channel system.

526 Figure 6. Schematic submarine-channel orientation pre (below) and post (above) diapir shortening.
527 Compare to Figure 4 RMS-amplitude maps.

528 Figure 7. Structural restoration. Early is at the bottom; present configuration is at the top. See text
529 for explanation.

530 Figure 8. Forward models of channel evolution based on different values of α (Eq. 4). From bottom
531 to top, decreasing α (increasing D , decreasing C_h) results in progressively larger meander
532 size and more translation of a high-curvature perturbation. See Supplementary Animation
533 1.

534 Figure 9. Comparison of forward model (A) to channel system between horizons 3-5 in the Campos
535 basin (B). Bends 1, 2, and 3 are comparable in parts A, B, and C. See Supplementary
536 Animation 2 for evolution of part A and Figure 5 for detailed geomorphologic and
537 stratigraphic character of the channel system in part B. (C) Plan-view patterns in parts A
538 and B are similar to observations of the Rio Mamoré from Google Earth Engine (Gorelick
539 et al., 2017).

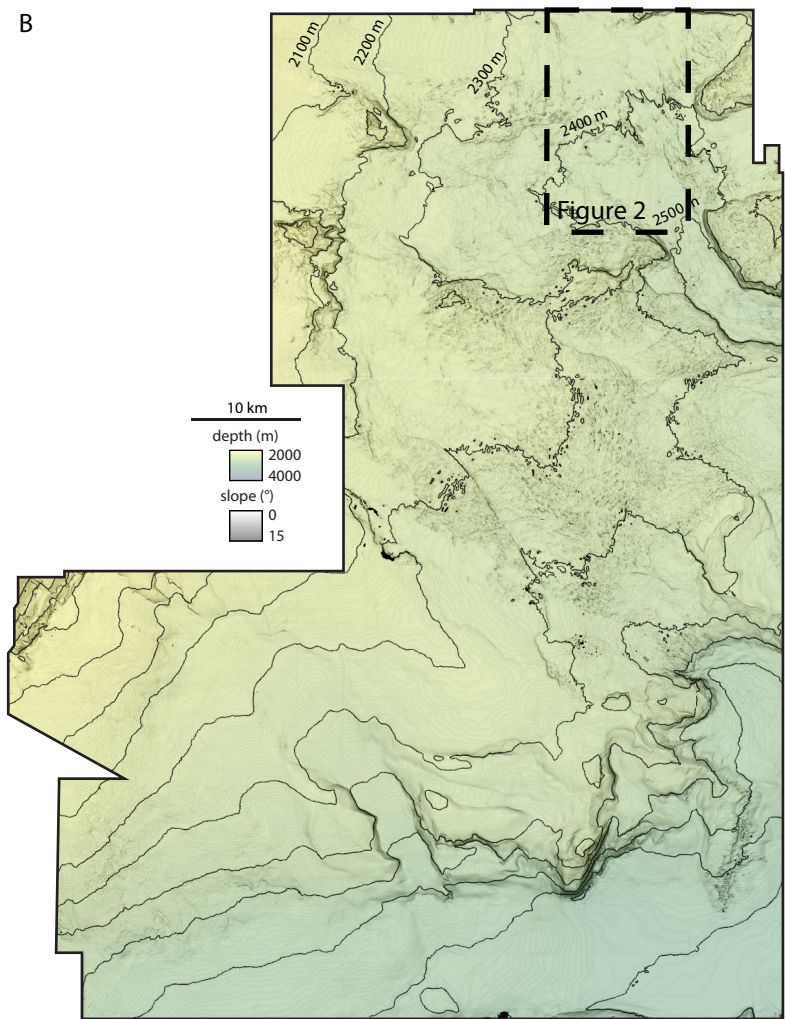
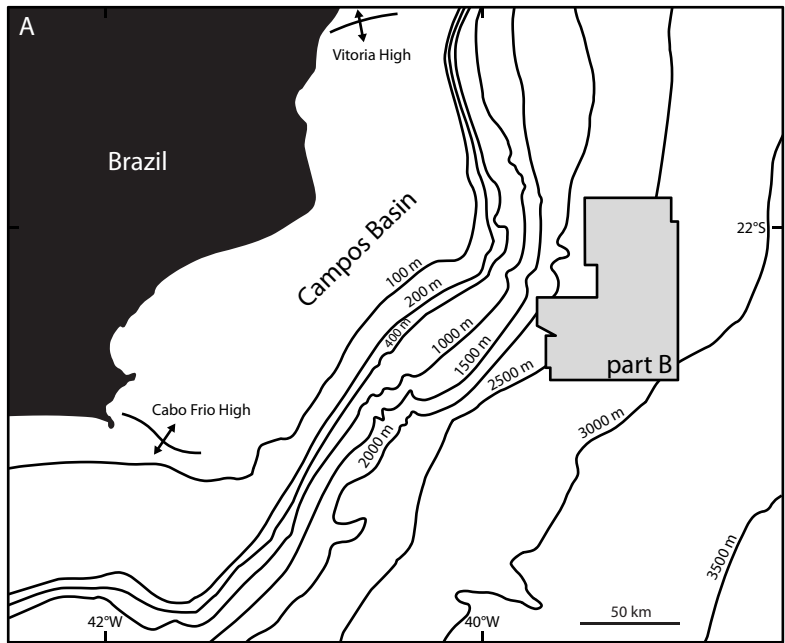


Figure 1.

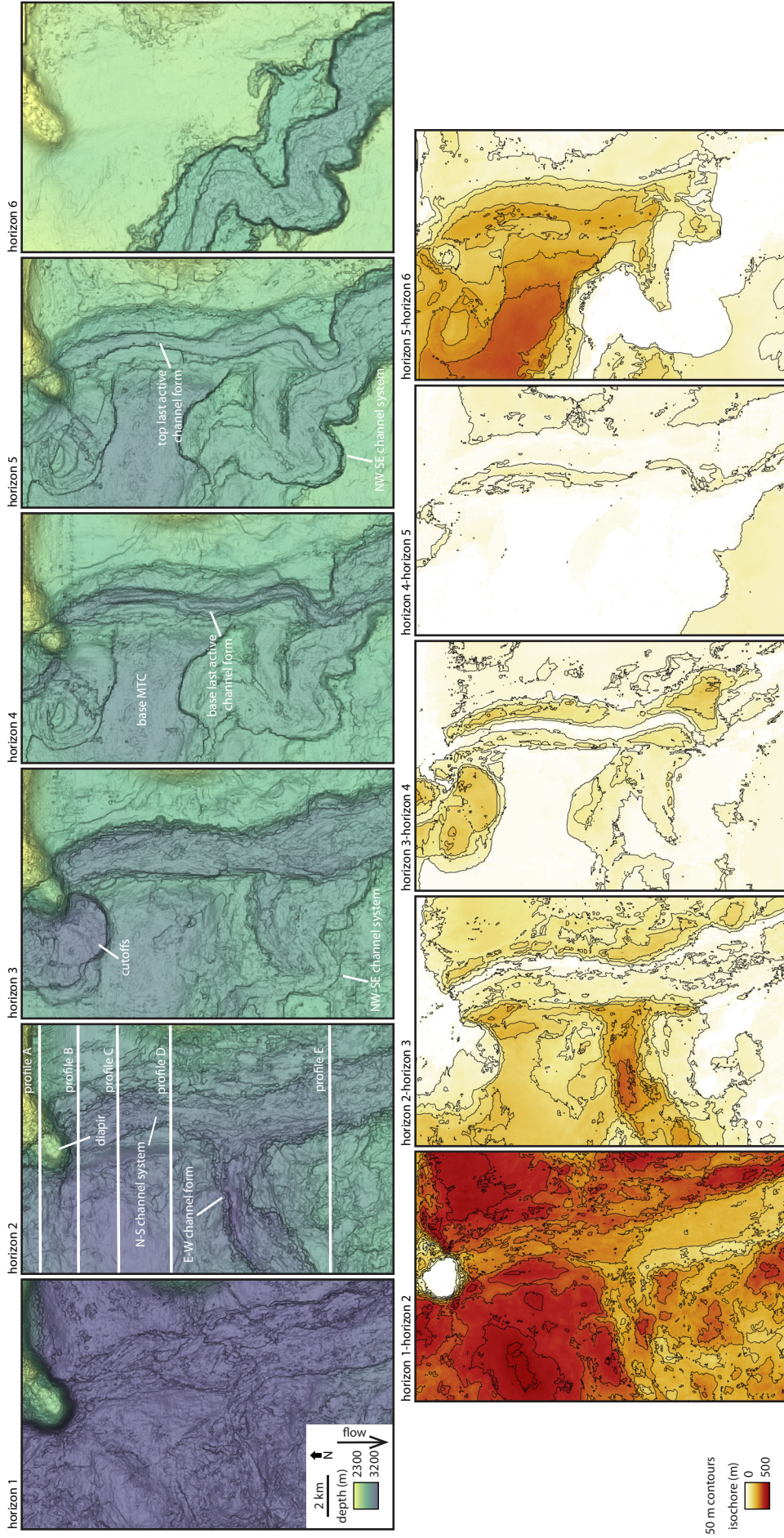


Figure 2.

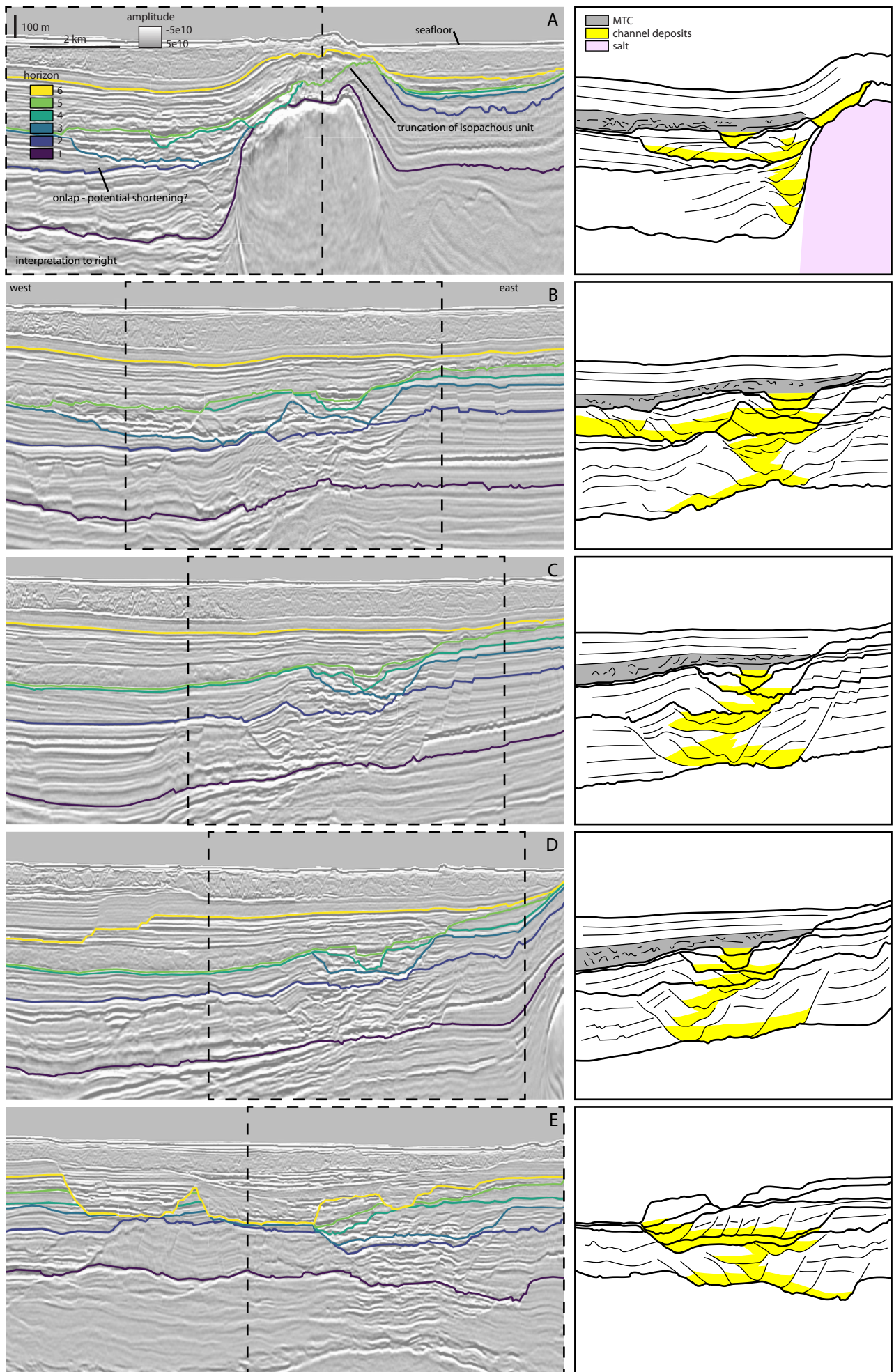


Figure 3

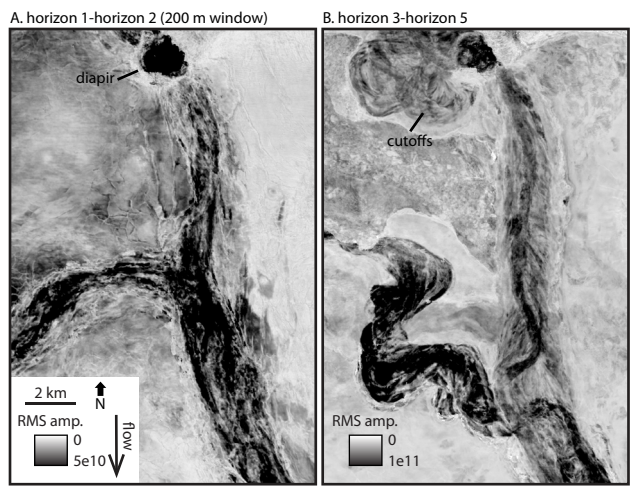


Figure 4.

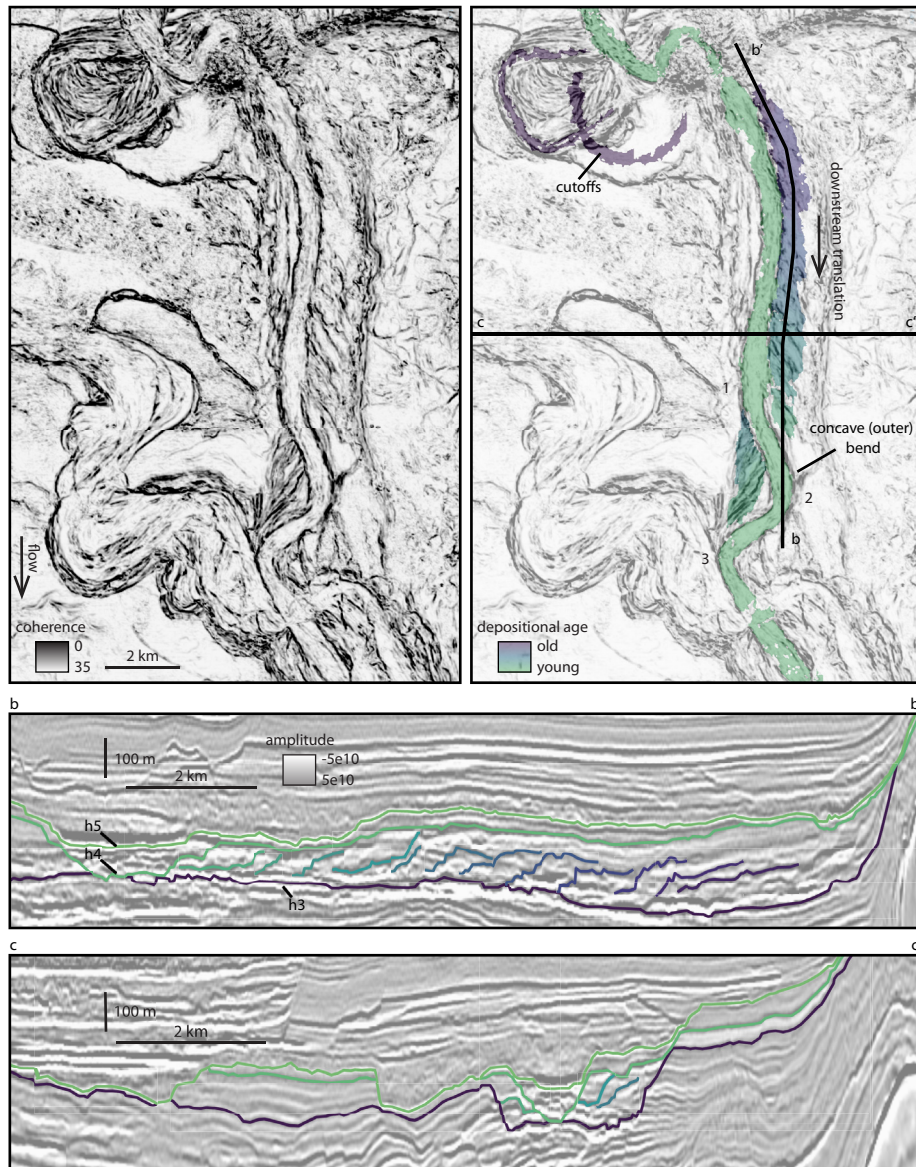
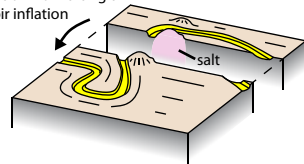


Figure 5.

A. schematic horizon 4-5 post shortening channel system

accommodation from tilting &
relative diapir inflation



B. schematic horizon 1-2 pre shortening channel system

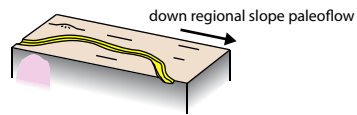


Figure 6.

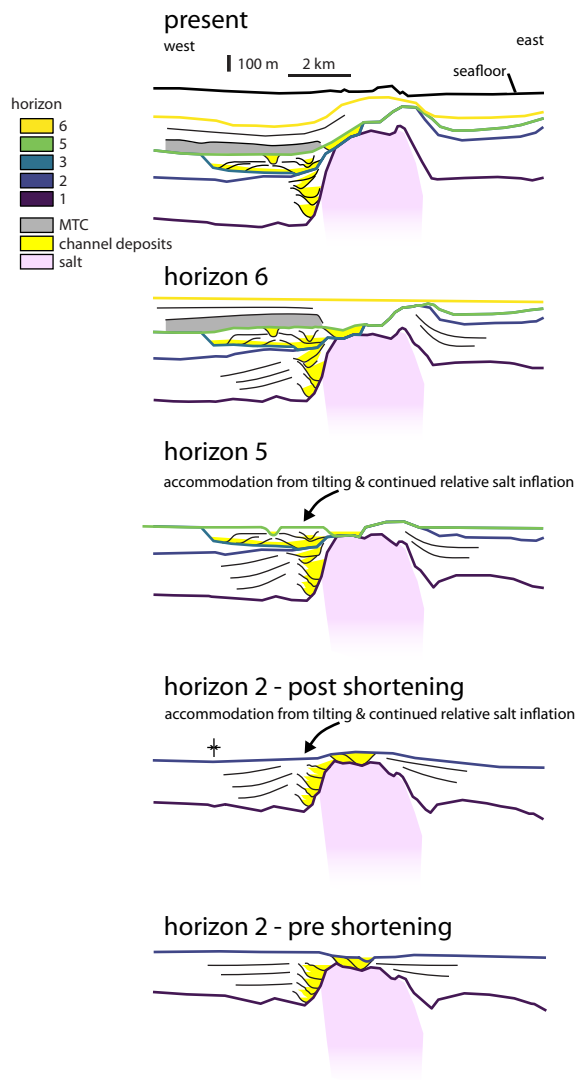
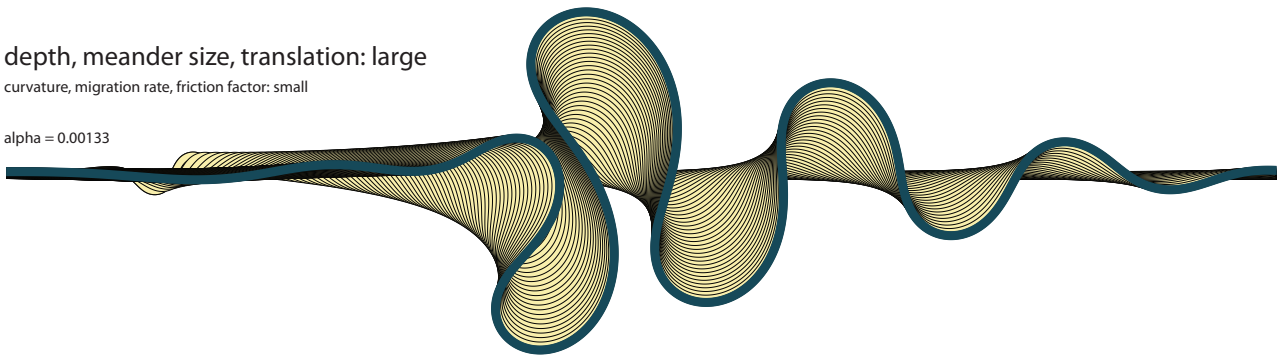


Figure 7.

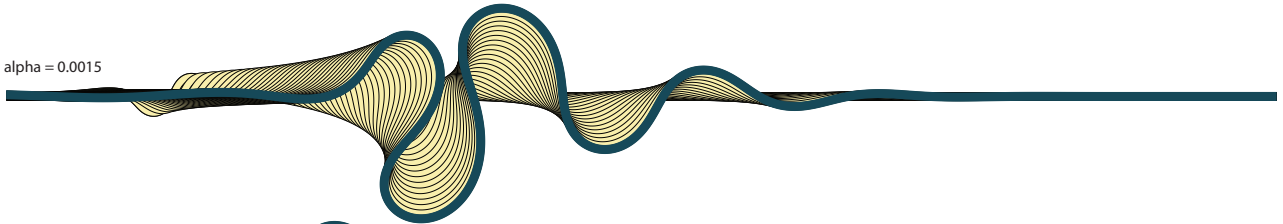
depth, meander size, translation: large

curvature, migration rate, friction factor: small

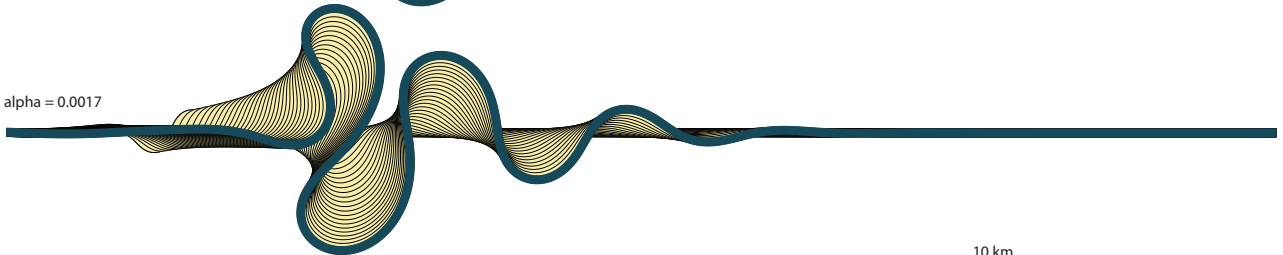
alpha = 0.00133



alpha = 0.0015



alpha = 0.0017



alpha = 0.002



alpha = 0.0024



alpha = 0.003



10 km

depth, meander size, translation: small

curvature, migration rate, friction factor: large

Figure 8.

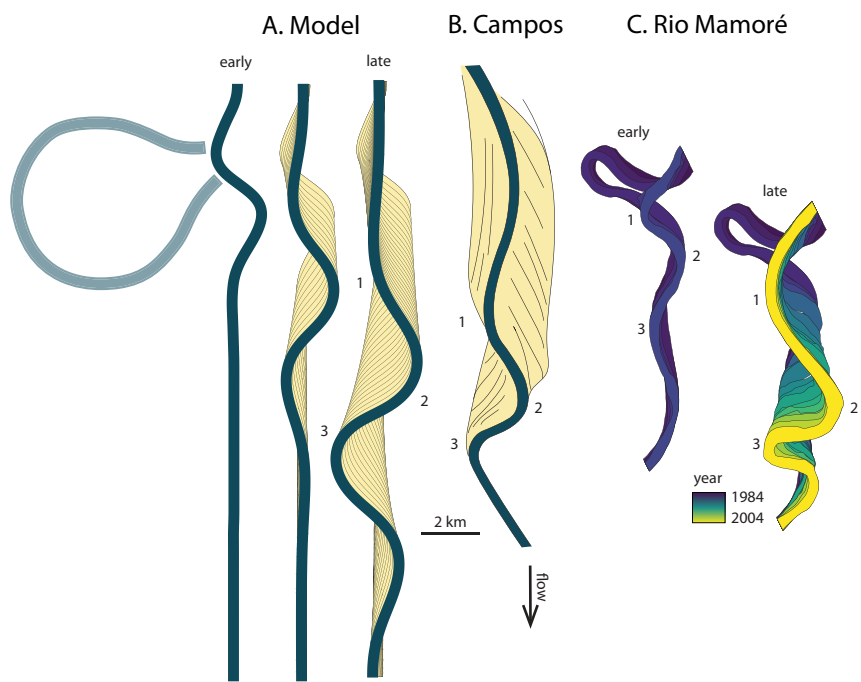


Figure 9.